

From surface to volume plasmons in hyperbolic metamaterials: General existence conditions for bulk high- k waves in metal-dielectric and graphene-dielectric multilayers

Sergei V. Zhukovsky,^{1,*} Andrei Andryeuskii,¹ J. E. Sipe,² and Andrei V. Lavrinenko¹

¹*DTU Fotonik, Department of Photonics Engineering, Technical University of Denmark, Ørsted Plads 343, DK-2800 Kgs. Lyngby, Denmark*

²*Department of Physics and Institute for Optical Sciences, University of Toronto, 60 St. George Street, Toronto, Ontario M5S 1A7, Canada*

We theoretically investigate general existence conditions for broadband bulk large-wavevector (high- k) propagating waves (such as volume plasmon polaritons in hyperbolic metamaterials) in subwavelength periodic multilayer structures. Describing the elementary excitation in the unit cell of the structure by a generalized resonance pole of a reflection coefficient, and using Bloch's theorem, we derive analytical expressions for the band of large-wavevector propagating solutions. We apply our formalism to determine the high- k band existence in two important cases: the well-known metal-dielectric, and recently introduced graphene-dielectric stacks. We confirm that short-range surface plasmons in thin metal layers can give rise to hyperbolic metamaterial properties, and demonstrate that long-range surface plasmons cannot. We also show that graphene-dielectric multilayers tend to support high- k waves and explore the range of parameters for which this is possible, confirming the prospects of using graphene for materials with hyperbolic dispersion. The approach is applicable to a large variety of structures, such as continuous or structured microwave, terahertz (THz) and optical metamaterials.

I. INTRODUCTION

Hyperbolic metamaterials (HMMs) are composite media that consist of subwavelength structures assembled so that an extreme anisotropy results on the macroscopic scale, with metallic behavior arising for one polarization of light and dielectric behavior for the other. In other words, their permittivity tensor $\epsilon = \text{diag}(\epsilon_x, \epsilon_y, \epsilon_z)$ has eigenvalues of different signs (e.g., $\epsilon_x = \epsilon_y < 0$ and $\epsilon_z > 0$ in the uniaxial geometry). Such anisotropy results in the dispersion relation in such a medium

$$\frac{\omega^2}{c^2} = \frac{k_x^2 + k_y^2}{\epsilon_z} + \frac{k_z^2}{\epsilon_{x,y}} \quad (1)$$

that is hyperbolic rather than elliptical (Fig. 1a), hence the name of HMMs. A hyperboloidal isofrequency surface is much more extended in the wave vector space than an ellipsoidal one – indeed, theoretically infinite in the idealization that Eq. (1) holds for all $k_{x,y,z}$ – so an HMM supports propagating solutions with very large wave vectors ($k^2 \gg \epsilon_{x,y,z} \omega^2 / c^2$). These waves, called high- k waves for short¹, would be extremely evanescent in any natural isotropic or weakly birefringent medium but become propagating in HMMs. The existence of high- k waves brings about a rich variety of new physics, both related to the waves themselves (as highly confined information carriers for subwavelength imaging²) and associated with a tremendous increase in the photonic density of states (PDOS) in HMMs, resulting in strong modification of all light-matter interaction phenomena that depend on it, such as spontaneous emission³.

What truly sparked the explosive scientific interest during the past few years was the discovery that HMM functionality can be exhibited in a non-resonant, broadband manner by structures with very simple geometry, such as nanorod arrays^{4,5} and metal-dielectric multilayers^{1,3}. An anomalous increase of the decay rate of nearby emitting centers (a broadband Purcell effect) was demonstrated experimentally^{1,5}, along with the direct measurement of radiation enhancement⁶. Many applications of HMMs have been suggested, such as far-

field subwavelength imaging or “hyperlensing”² and highly absorptive surfaces that benefit (rather than suffer) from increased roughness⁷. More fundamental and more intriguing uses for HMMs have also been envisaged, exploiting mathematical similarities between sign changes in the dispersion relation (1) and metric signature transitions in cosmological equations^{8,9}. Many more areas of research are being explored, as can be seen in the recent reviews^{10,11} and references therein.

Even though the effective permittivity representation of HMMs has proved very successful in predicting and explaining their exotic physics, it is the high- k waves that govern the functioning of any HMM on a microscopic level. Hence it is these waves that eventually determine the extents and limits of applicability of a particular HMM with respect to any of the effects described above. Thus, it is crucial to understand the physical nature of these waves. In metal-dielectric structures, the conventional wisdom is that the nature is plasmonic, so various groups have chosen different terms for them: *multilayer plasmons*¹², *Bloch plasmon polaritons*¹³, or *volume plasmon polaritons* (VPPs)^{11,14}. In HMMs with a multilayer geometry, VPPs should arise from coupling of surface plasmon polaritons (SPPs) at layer interfaces^{15–17}. In our recent work¹⁸, we showed explicitly that VPPs originate from coupling of short-range SPPs (SRSPPs) in individual metal layers by keeping only the SRSPP response in these layers via a pole expansion. It is noteworthy that an SRSPP exists for just one value of the wave vector, whereas the resulting VPPs exist in the entire range of them, spanning the isofrequency surface in Fig. 1c.

Two interesting observations were made alongside this proof. First, it appeared that there is a stark contrast between the two characteristic excitations in the metal layer: the short-range SPP capable of giving rise to HMM behavior, and the long-range SPP (LRSPP) that do not have such a capability. Second, as also mentioned in other accounts¹⁹, VPPs were shown to exist outside of the HMM regime, albeit in a somewhat narrower band in the wave vector space. The general principle, namely, “lower-dimensional elementary unit cell

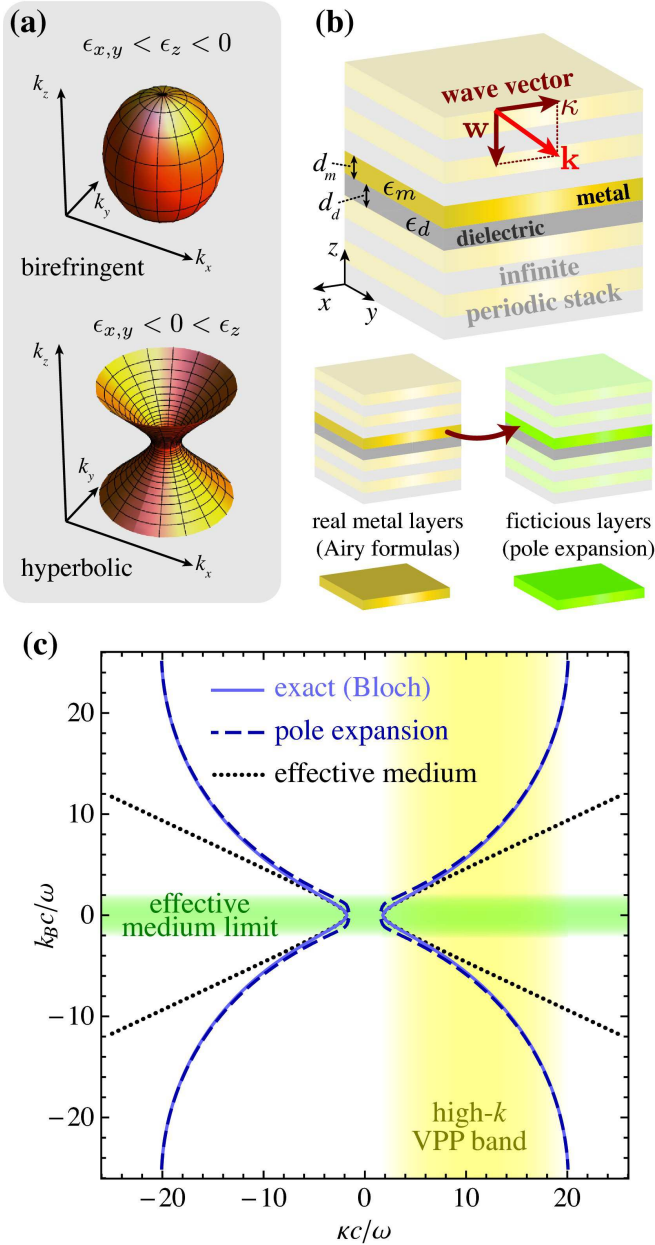


Figure 1. (Color online) Theoretical background on hyperbolic metamaterials (HMMs). (a) Isofrequency surfaces in the dispersion relation [Eq. (1)] for conventional anisotropic medium ($\epsilon_{x,y,z} > 0$) and HMM ($\epsilon_{x,y} < 0$ and $\epsilon_z > 0$). (b) An infinite periodic multilayer HMM with geometric notations and wave vector decomposition used in the paper, along with the illustration of the replacement of real metal layers with reflection and transmission coefficients given by Eq. (3) with fictitious layers featuring just a pole-like elementary excitation with reflection and transmission coefficients given by Eq. (8). (c) Comparison between the actual multilayer dispersion relation [Eq. (6)], the dispersion relation derived from the pole expansion [Eq. (9)], and the effective-medium dispersion relation [Eq. (1) with Eq. (7)] for the structure with layer thicknesses $d_m = 2.3$ nm, $d_d = 11.4$ nm and permittivities $\epsilon_m = -17.2$, $\epsilon_d = 2.59$ (relevant for Au/Al₂O₃ structures for $\lambda = 715$ nm¹). The yellow shaded area shows the band of propagating high- k VPPs.

excitations coupling form a higher-dimensional excitation in a periodic arrangement of such cells” is undoubtedly behind the formation of VPPs in multilayer HMMs. Nevertheless, it still remains to be determined what conditions these elementary excitations must satisfy to form a high- k band spanning a broad range of k , such as happens in VPPs. A general understanding would be very useful in determining the applicability range for new types of HMMs, such as, for example, graphene-based multilayers introduced in recent works^{20–23}.

In this paper, we theoretically investigate general existence conditions for broadband bulk high- k propagating waves (such as VPPs in HMMs) in arbitrary periodic multilayers structures. We treat the elementary excitation in the unit cell of such a structure as a generalized resonance defined by a pole-like response in its Fresnel reflection and transmission coefficients. Then, using Bloch’s theorem, we derive analytical expressions for the band of high- k propagating solutions that can originate from this elementary excitation by hybridization in the periodic structure. Using these analytical expressions, we show that SRSPPs in thin metal layers can – and commonly do – give rise to HMM-like properties in subwavelength metal-dielectric multilayers; on the other hand, LRSPPs only form a very narrow plasmonic band near the light line of the dielectric and do not produce a high- k band. Furthermore, we apply the formalism to graphene-dielectric metamaterials in the THz range. We show that TM-polarized plasmons in individual graphene sheets also hybridize to form VPPs with HMM-like properties in the frequency range where the imaginary part of the graphene conductivity significantly exceeds its real part. On the other hand, *transverse* or TE-polarized graphene plasmons^{24,25} behave like LRSPPs in metal-dielectric multilayers, not giving rise to HMM-like behavior.

The present results are primarily valuable from the theoretical point of view, providing a general understanding of how high- k band of bulk propagating waves originate from fixed- k surface excitations in individual layers of a multilayer system. In addition, our results have practical applications, allowing for very efficient estimation of VPP dispersion and HMM properties in existing HMMs (metal-dielectric and graphene-dielectric multilayers), which is useful in the design of HMM-based devices such as hyperlenses with improved performance. Moreover, the present results provide a means to determine whether any localized excitation (electromagnetic or otherwise) is likely to give rise to HMM-like or bulk plasmon-like behavior when assembled into a periodic system. Examples may include optical waveguide arrays, multilayers supporting Bloch surface waves or spoof surface plasmons, periodic layers of two-dimensional electron gas (e.g. multiple quantum-well semiconductor heterostructures) or even acoustic multilayers.

This paper is organized as follows. Section II briefly reviews the basic theoretical background on multilayer HMMs, including the dispersion relation for the VPPs and its representation using the pole expansion formalism¹⁸. In Section III we analyze this representation and derive the existence conditions for broad VPP band formation from arbitrary resonant elementary excitation in the metamaterial’s unit cell. In Section

IV we apply our findings to several cases of pole expansion, including multilayers made of metal and graphene; specifically, we show that short-range SPPs do give rise to HMM behavior while long-range SPPs do not. We also analyse the applicability of graphene for high- k HMMs. Finally, in Section V we summarize the results.

II. VOLUME PLASMON POLARITONS IN MULTILAYER HYPERBOLIC METAMATERIALS

We begin by recalling that in an infinite, periodic metal-dielectric structure (Fig. 1b) where losses are neglected, and so metal layers with permittivity $\epsilon_m < 0$ and thickness d_m alternate with dielectric layers with permittivity $\epsilon_d > 0$ and thickness d_d , the dispersion relation of propagating waves can be obtained via Bloch's theorem using the standard transfer matrix approach²⁶. From the transfer matrix for one period of the structure,

$$M_1 = \frac{1}{T_m} \begin{bmatrix} T_m^2 - R_m^2 & R_m \\ -R_m & 1 \end{bmatrix} \begin{bmatrix} e^{i w_d d_d} & 0 \\ 0 & e^{-i w_d d_d} \end{bmatrix}, \quad (2)$$

where the reflection and transmission coefficients of a metal layer R_m and T_m are given by the Airy formulas,

$$R_m = r_{dm} + \frac{t_{dm} r_{md} t_{md} e^{2i w_m d_m}}{1 - r_{md}^2 e^{2i w_m d_m}}, \quad T_m = \frac{t_{dm} t_{md} e^{i w_m d_m}}{1 - r_{md}^2 e^{2i w_m d_m}}, \quad (3)$$

the interface reflection and transmission coefficients given by the Fresnel formulas,

$$\begin{aligned} r_{md} &= \frac{w_m \epsilon_d - w_d \epsilon_m}{w_m \epsilon_d + w_d \epsilon_m}, \quad r_{dm} = \frac{w_d \epsilon_m - w_m \epsilon_d}{w_d \epsilon_m + w_m \epsilon_d}, \\ t_{md} &= \frac{2 w_m \sqrt{\epsilon_m \epsilon_d}}{w_m \epsilon_d + w_d \epsilon_m}, \quad t_{dm} = \frac{2 w_d \sqrt{\epsilon_d \epsilon_m}}{w_d \epsilon_m + w_m \epsilon_d}, \end{aligned} \quad (4)$$

and

$$w_m = \sqrt{\epsilon_m \omega^2 / c^2 - \kappa^2}, \quad w_d = \sqrt{\epsilon_d \omega^2 / c^2 - \kappa^2}, \quad (5)$$

expressing the relation between the tangential (κ) and the normal (w) component of the wave vector in each layer (we choose the square root of complex w_j so that $\text{Im } w_j \geq 0$; if $\text{Im } w_j = 0$ we take $\text{Re } w_j \geq 0$), Bloch's theorem yields^{15,17,27}

$$\begin{aligned} \frac{\text{Tr } M_1}{2} &= \cos[k_B(d_m + d_d)] = \cos(w_m d_m) \cos(w_d d_d) \\ &\quad - \frac{1}{2} \left(\frac{\epsilon_m w_d}{\epsilon_d w_m} + \frac{\epsilon_d w_m}{\epsilon_m w_d} \right) \sin(w_m d_m) \sin(w_d d_d). \end{aligned} \quad (6)$$

This expression describes a propagating Bloch wave with tangential component κ and normal component k_B . To relate it to the hyperbolic dispersion relation (1), one can Taylor expand it around the points where $\cos[k_B(d_m + d_d)] = 1$. Provided the layers are thin enough ($d_m, d_d \ll \lambda$) so that $w_j d_j \ll 1$, Eq. (6) reduces to $\omega^2 / c^2 = k_B^2 / \epsilon_{x,y} + \kappa^2 / \epsilon_z$ ¹², similar to Eq. (1) where $k_B = k_z$, $\kappa^2 = k_x^2 + k_y^2$, and

$$\epsilon_x = \epsilon_y = \frac{d_m \epsilon_m + d_d \epsilon_d}{d_m + d_d}, \quad \epsilon_z^{-1} = \frac{d_m \epsilon_m^{-1} + d_d \epsilon_d^{-1}}{d_m + d_d}, \quad (7)$$

which results in $\epsilon_x = \epsilon_y < 0$ and $\epsilon_z > 0$ in a broad range of parameters.

As seen in Fig. 1c, the Bloch waves in HMMs approach a hyperbolic dispersion relation for smaller κ but deviate from it as κ increases. The upper limit $\kappa_{\text{max}} \propto 1/(d_m + d_d)$ ²⁸ is a cut-off imposed by the finite thickness of constituent layers, fundamentally limiting the applicability of the effective medium approximation. This cut-off, essentially resulting from violation of the subwavelength condition for waves with very large κ , is the primary limiting factor for the overall PDOS increase in multilayer HMMs. Another limitation is related to the presence of losses¹¹, which would also eventually render the Bloch waves fully evanescent. Yet another, more fundamental limitation is associated with the non-local effects in the response of the electron gas in metal²⁹.

Finally, to relate the Bloch waves given by Eq. (6) to VPPs, one can replace the metal layers with a hypothetical structure whose reflection and transmission coefficients only contain one resonant guided-wave excitation, i.e., are of the form of a simple pole¹⁸

$$T_m = \frac{\tau}{\kappa - \kappa_p}, \quad R_m = \frac{-\tau}{\kappa - \kappa_p} - \frac{\tau}{\kappa_p}, \quad (8)$$

where the location of the pole κ_p and the pole strength τ depend on the exact nature of the excitation. Practically, for the case of metal-dielectric multilayers one can determine τ and κ_p by comparing the generalized form of reflection and transmission coefficients Eq. (8) to the Airy formulas (3). The second term in the expansion for R_m is to ensure that $R_m = 0$ for $\kappa \rightarrow 0$, as normally incident light should be incapable of exciting any guided wave in a planar layer due to momentum conservation.

Calculating the values of κ_p and τ for the SRSPP in a thin metal layer, and substituting Eq. (8) rather than Eq. (3) into Eq. (2), one obtains a modified form of the dispersion relation¹⁸,

$$\cos[k_B(d_m + d_d)] \approx \left[1 - \frac{\kappa - \kappa_p}{2\tau} \right] e^{i w_d d_d} + \frac{\kappa - \kappa_p}{2\tau} e^{-i w_d d_d}, \quad (9)$$

which is seen to correspond to the exact dispersion relation of the multilayer very closely (Fig. 1c), correctly describing high- k waves in such a multilayer. Hence, it can be concluded that these waves originate from hybridization of SRSPPs in the metal layers, and are indeed VPPs. We note that these VPPs exist in a very wide range of κ while the original SPPs only exist at a single $\kappa = \kappa_p$. It is somewhat surprising that VPP formation is specific to SRSPPs; other pole-like excitations present in a thin metal layer, such as the LRSPP, was not found to affect the VPP band in any significant way. Another interesting observation was that VPPs were found to exist *outside* of the HMM range¹⁸, where earlier works indeed predicted two branches of propagating waves, one with positive and one with negative refraction¹⁹. However, the range of the VPP band in this regime was found to be significantly narrower in κ , and Eq. (1) was no longer applicable.

All these facts taken together mean that it is necessary to understand whether and when a pole-like excitation of the

type of Eq. (8) leads to the formation of a VPP band which would be sufficiently broadband to lead to an HMM response. This understanding, in the form of generalized existence conditions for the VPP band, is especially important for predicting whether an HMM regime is possible with new types of plasmonic multilayer structures, such as those based on graphene, and what prevents other kinds of structures, such as high-index dielectric waveguide arrays, from giving rise to HMM properties.

III. FORMATION OF LARGE-WAVEVECTOR BAND

We begin our investigation by using Eq. (8) and rederiving the dispersion relation in the general form,

$$\cos[k_B(d_m + d_d)] = \frac{\kappa - \kappa_p}{2\tau} e^{\frac{2\pi d}{\lambda} \sqrt{\kappa^2 - \epsilon_d}} - \left[\frac{\tau}{\kappa_p} + \left(\frac{\tau}{\kappa_p} \right)^2 \frac{\kappa - \kappa_p}{2\tau} \right] e^{-\frac{2\pi d}{\lambda} \sqrt{\kappa^2 - \epsilon_d}} \equiv F(\kappa), \quad (10)$$

where τ , κ and κ_p are now dimensionless (normalized by $\omega/c = 2\pi/\lambda$).

The existence condition for propagating waves will then be $F(\kappa) \in [-1; 1]$, and in order to better analyze it, we introduce several dimensionless quantities:

$$\xi \equiv \frac{\tau}{\kappa_p}, \quad \eta \equiv \frac{2\pi d}{\lambda}, \quad \chi \equiv \frac{\sqrt{\epsilon_d}}{\kappa_p}, \quad \text{and} \quad \beta \equiv \frac{\kappa}{\kappa_p}. \quad (11)$$

We see that η is the measure of how “subwavelength” the spacer dielectric layers appear to be with respect to the vacuum wavelength of the incident light (so normally $\eta \ll 1$); χ indicates the position of the dielectric cut-off (point on the light line for a given frequency) normalized to the position of the pole (again, $\chi \ll 1$ and can be neglected unless κ_p is very close to the light line, e.g., for LRSPPs); ξ characterizes the pole strength (and nothing will be assumed about it; note that Eq. (9) results from Eq. (10) for $\xi \rightarrow -1$); and β is the tangential component of the wavevector normalized to the position of the pole. Using these quantities, we can rewrite Eq. (10) in a more symmetric way,

$$\frac{1}{2}(\beta - 1)A(\beta) - \frac{1}{2}(\beta + 1)A^{-1}(\beta) \equiv F(\beta) \in [-1; 1], \quad (12)$$

where

$$A = \xi^{-1} \exp\left(\eta \kappa_p \sqrt{\beta^2 - \chi^2}\right). \quad (13)$$

We can now analyze the limiting cases of Eq. (12). For the combination of parameters such that $A \gg 1$ (achieved for significantly large κ_p and/or very small ξ), one can neglect the term with A^{-1} and see that $F(\beta) = \pm 1$ can be solved analytically to yield

$$\beta = 1 + (\eta \kappa_p)^{-1} W(\pm 2\xi \eta \kappa_p e^{-\eta \kappa_p}), \quad (14)$$

where $W(z)$ is the Lambert W function³⁰ defined as the solution of $W(z)e^{W(z)} = z$. If its argument is small, we can use the

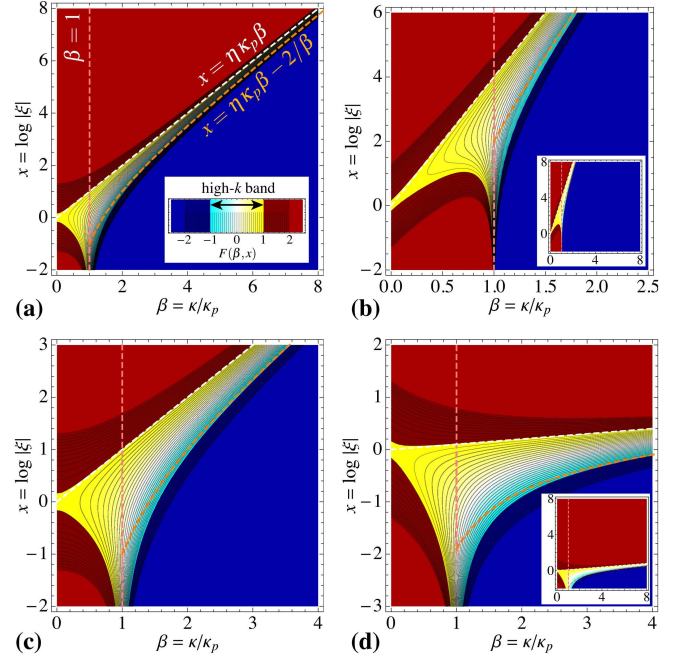


Figure 2. (Color online) Behavior of Eq. (12) in different regimes. (a) Illustration of the limiting behavior of $F(\beta, x = \log|\xi|)$ for large β and x ; the dashed lines show the asymptotes given by Eqs. (15)–(16). (b–d) An enlarged view of $F(\beta, x)$ around the asymptote intersection point ($\beta = 1, x = \eta\kappa_p$) for $\eta\kappa_p$ equal to (b) 4, (c) 1, and (d) 0.1. The insets show the plots in (b) and (d) in the same scale as (a) for comparison.

first-order approximation $W(z) \approx z$ to yield that VPPs exist if

$$\beta \in [1 - 2\xi e^{-\eta\kappa_p}; 1 + 2\xi e^{-\eta\kappa_p}]. \quad (15)$$

So, there should be a VPP band around $\beta = 1$ (i.e., $\kappa = \kappa_p$), which is usually narrow unless $\eta\kappa_p$ is small. This explains that the VPP band should widen as the structure becomes more subwavelength (smaller η), but does not explain how it can fill a very broad range of κ since that would require violating the assumptions leading to Eq. (15). Additionally, we see that $\beta = 1$ represents the limiting behavior of Eq. (12) for very small ξ .

The other limit can be obtained by noticing that for the case of $A = A^{-1} = 1$, we have $F(\beta) = -1$ regardless of any other parameters. Changing to the logarithmic scale with respect to ξ by defining $x \equiv \ln|\xi|$, we see that the dependence

$$x = \eta \kappa_p \beta \quad \text{where} \quad e^x = |\xi| \quad (16)$$

is likely to describe the edge of another VPP band. Indeed, if the argument of the exponent in Eq. (13) is small enough so that $A^{\pm 1} \approx 1 \pm (\eta \kappa_p \beta - x)$, then it follows that $F(\beta) = 0$ for $x = \eta \kappa_p \beta - 1/\beta$ and $F(\beta) = 1$ for $x = \eta \kappa_p \beta - 2/\beta$. Hence Eq. (16) describes the second limiting case for the existence of the VPP band, which is narrow for large ξ (and β) and becomes wider as ξ decreases.

This limiting case analysis can be used to easily predict the existence of the VPP band in the (β, x) space, as seen in

Fig. 2a. We see that the VPP band follows the line $\beta = 1$ until $x = 0$, after which it slants to follow the line $\beta = x/(\eta\kappa_p)$. The VPP bands corresponding to the two asymptotes overlap near the intersection point ($\beta = 1, x = \eta\kappa_p$), where the equation ceases to be analytically solvable and the VPP band has a more complicated shape (Fig. 2b–d). It was also established that non-zero ζ influences this behavior only weakly, suppressing any solutions of Eq. (12) below the light line ($\beta \leq \chi$) and slightly modifying the limiting behavior near it.

We can thus identify two distinct characteristic cases when the VPP band is sufficiently broad. First, it can be seen that for the both limiting cases, the band widens as ξ approaches unity (Fig. 2). Hence the region $0.1 \leq \xi \leq 10$ corresponds to the case when bulk propagating solutions are supported for the widest range of κ . Second, for the special case $\eta\kappa_p \ll 1$, when the line corresponding to Eq. (16) is nearly horizontal, there is a narrow range of $x \in [-2/\beta; 0]$ when the VPP band width spans from below unity all the way to $\sqrt{2/(\eta\kappa_p)}$, approaching very large values for $x \rightarrow -0$ for very deeply sub-wavelength structures.

IV. EXAMPLES

A. SRSPP and LRSPP in metal-dielectric stacks

The most straightforward way to test the proposed criteria is to apply the conditions to the well-studied HMM produced from metal-dielectric multilayers, using SPPs in the metal layers as the elementary excitations in Eq. (8). It is known that a metal layer supports two types of such plasmons depending on whether the individual plasmons at the layer interfaces are coupled symmetrically or antisymmetrically with respect to the dominant field component E_z . Both these modes can be obtained from the equation

$$1 - r_{md}^2 \exp(2i\omega_m d_m) = 0. \quad (17)$$

The primary difference between them is the behavior of their propagation constant κ_p as the metallic layer thickness d_m approaches zero. The symmetrically coupled SPP has its wave vector approach the light cone ($\kappa_p \rightarrow \sqrt{\epsilon_d}$), and if the metal is lossy, the losses decrease as the wave becomes increasingly less confined to the layer. The asymmetrically coupled SPP has its wave vector approach infinity ($\kappa_p \rightarrow \infty$), and the wave becomes increasingly more confined to the metal layer, so the losses increase. For the latter reason, these two SPPs are traditionally denoted long-range and short-range, or LRSPP and SRSPP, respectively.

It has already been proved¹⁸ that SRSPPs can and do give rise to the VPP band in metal-dielectric HMMs, and we begin by reproducing this result with the proposed criteria. In the appropriate limit of sufficiently thin metal layer, the expressions for the pole expansion parameters for Eq. (8) can be obtained from Eq. (17) as, in dimensionless units,

$$\kappa_p = \frac{\log|r|}{2\pi d_m/\lambda}, \quad \tau = \frac{r^{-1} - r}{2(2\pi d_m/\lambda)}, \quad r = \lim_{\kappa \rightarrow \infty} r_{md} = \frac{\epsilon_m - \epsilon_d}{\epsilon_m + \epsilon_d}. \quad (18)$$

We note at once that ξ does not depend on d_m , making the analysis particularly easy:

$$\xi = \frac{r^{-1} - r}{2 \log|r|} = \frac{2f}{(f^2 - 1) \log \left| \frac{1+f}{1-f} \right|}, \quad (19)$$

where $f = -\epsilon_d/\epsilon_m$. We can see that $\xi \gtrsim 1$ unless $f \rightarrow 1$ (Fig. 3a). So, it can be concluded that broadband VPPs are commonly formed by hybridization of SRSPPs, as confirmed by the example in Fig. 3b. The only exception is when $\epsilon_m + \epsilon_d \approx 0$ leading to $|\xi| \gg 1$, so the VPP band becomes increasingly more narrow-band and moves towards larger κ (see the inset in Fig. 2a). Note that this corresponds to an epsilon-near-zero (ENZ) regime rather than an HMM regime according to Eqs. (7), and the narrowing and shifting of the VPP band near the ENZ points is consistent with our earlier observation¹⁸. The VPP band shift remains small since the slope parameter, $\eta\kappa_p = (d_d/d_m) \log|r|$, becomes very large in the ENZ case.

On the other hand, the LRSPP is obtained from Eq. (17) by considering the other limit ($\kappa_p \rightarrow \sqrt{\epsilon_d}$). The resulting expressions are

$$\kappa_p = \sqrt{\epsilon_d + (\epsilon_d - \epsilon_m) \frac{\epsilon_d^2}{\epsilon_m^2} \left(\frac{1-\delta}{1+\delta} \right)^2}, \quad (20)$$

$$\tau = \frac{\epsilon_d - \epsilon_m}{2\kappa_p} \frac{\epsilon_d^2}{\epsilon_m^2} \frac{(\delta-1)^2}{\delta(\delta+1)}, \quad \delta = e^{-d_m \sqrt{(\epsilon_d - \epsilon_m)}},$$

which gives

$$\xi = \frac{(\epsilon_d - \epsilon_m) \epsilon_d^2 / \epsilon_m^2}{\epsilon_d + (\epsilon_d - \epsilon_m) \frac{\epsilon_d^2}{\epsilon_m^2} \left(\frac{1-\delta}{1+\delta} \right)^2} \frac{(\delta-1)^2}{\delta(\delta+1)}, \quad (21)$$

and it can be seen that $\xi \rightarrow 0$ as $d_m \rightarrow 0$ and the structure becomes increasingly more subwavelength. This means that LRSPPs hybridize to form but a very narrow band around κ_p according to Eq. (15) (Fig. 2a), and thus do not contribute to the VPP band. This is seen in Fig. 3a, and further demonstrated by comparing the location of the area given by $-1 < F(\beta, x) < 1$ in the (β, x) coordinates for the characteristic metal-dielectric multilayers (Fig. 3b) and the dispersion of VPPs in the bands (Fig. 3c) for LRSPP vs. SRSPP cases. This result can also be explained by noting that an LRSPP in a metallic layer bears more and more resemblance to a plane wave in the surrounding medium as the layer becomes thinner, which is accompanied by progressively poorer coupling between the wave and the metal; it is this poor coupling that manifests itself in $\xi \rightarrow 0$. The same poor coupling will thus be characteristic for VPPs resulting from LRSPPs, which will therefore be very similar in properties to plane waves propagating in the dielectric of the HMM and thus occupy but a very narrow range of κ .

On the other hand, for ξ to be on the order of unity in the LRSPP case, the quantity $2\pi d_m/\lambda$ needs to be between 0.25 and 1 (see Fig. 3d), i.e., the multilayer should not be very subwavelength. In this regime, it can be expected that both LRSPPs and SRSPPs may contribute to the VPP band,

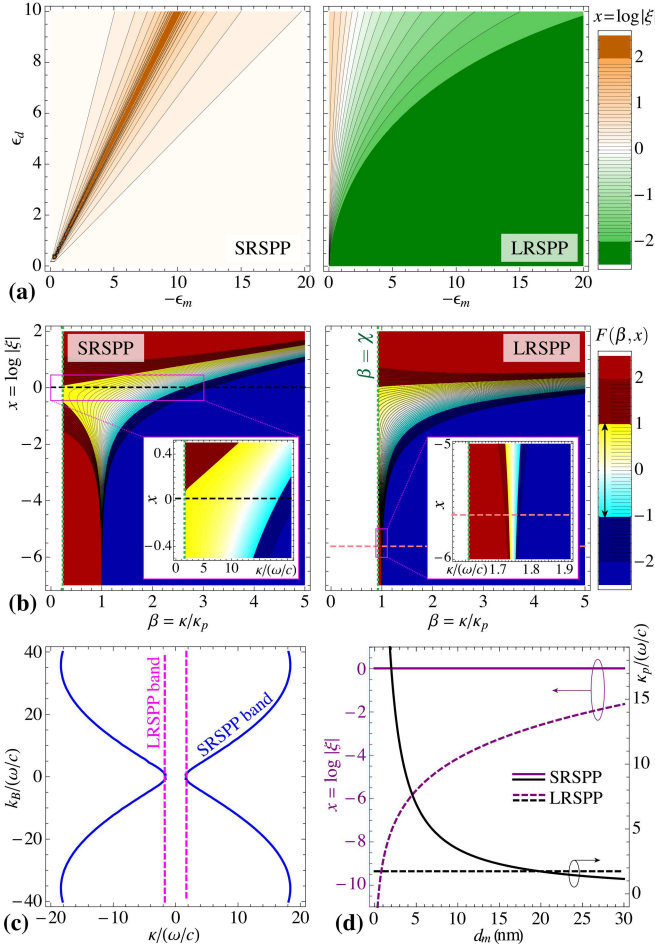


Figure 3. (Color online) Formation of the VPP band in metal-dielectric HMMs from SRSPPs and LRSPPs. (a): Dependence of x on the permittivities of metal and dielectric in a thin metal layer ($d_m = 5$ nm) for SRSPPs and LRSPPs. (b) Example dependencies of $F(\beta, x)$ for SRSPP and LRSPP in a structure with $d_m = d_d = 5$ nm and material parameters as in Fig. 1c. The insets show the enlarged view in the scale of $\kappa_p/(\omega/c)$. (c-d) Comparison between SRSPP and LRSPP case for (c) the dispersion relation of the VPP band and (d) the dependence of κ_p and x on d_m .

in line with the recent observation that real multilayer structures can outperform ideal HMMs for some values of layer thicknesses^{28,31}.

B. Graphene-dielectric multilayers

Besides metallic layers, plasmonic excitations are present in other thin-film structures such as monolayered graphene, and it has been proposed that separating graphene layers by dielectric spacers and combining them into multilayers³² can give rise to a new type of HMMs, predominantly in the THz range^{20–23}. Here we apply our approach to analyze the pre-requisites needed for a VPP band formation.

Graphene can be regarded as an infinitely thin sheet with surface conductivity σ . In the THz to far infrared (far-IR)

range for graphene Fermi energy $E_F > k_B T$, it can be calculated according to the Kubo approach with the formula³³

$$\sigma = i \frac{e^2 k_B T}{\pi \hbar^2} \left[\frac{E_F}{k_B T} + 2 \ln \left(1 + e^{-\frac{E_F}{k_B T}} \right) \right] \frac{1}{\omega + i\gamma} + i \frac{e^2}{4\pi \hbar} \ln \frac{2|E_F| - \hbar(\omega + i\gamma)}{2|E_F| + \hbar(\omega + i\gamma)} \quad (22)$$

where T is the temperature and γ is the damping rate, which depends on the quality of graphene. The first and the second terms in Eq. (22) corresponds to interband and intraband contributions, respectively. The resulting conductivity (real and imaginary part) is shown in Fig. 4(a)–(b). We see that the imaginary part $\text{Im } \sigma > 0$, which corresponds to “metal-like” behavior of graphene, everywhere except in a narrow region of frequencies and electrochemical potential [white area close to the dashed line in Fig. 4 (b)]. As with the metal-dielectric multilayers, we will neglect losses here, considering the frequency range where the real part of σ is small, and will assume that σ is purely imaginary.

Surrounding a sheet of graphene with conductivity σ by dielectric with permittivity ϵ , the transmission coefficient for the TM polarization is given by³⁴

$$T = \frac{2\epsilon/\sqrt{\epsilon - \kappa^2}}{2\epsilon/\sqrt{\epsilon - \kappa^2} + (Z_0 \sigma)}, \quad (23)$$

where $Z_0 = 1/(\epsilon_0 c) \approx 377 \Omega$ is the impedance of free space. Assuming for now that there are no losses in graphene and

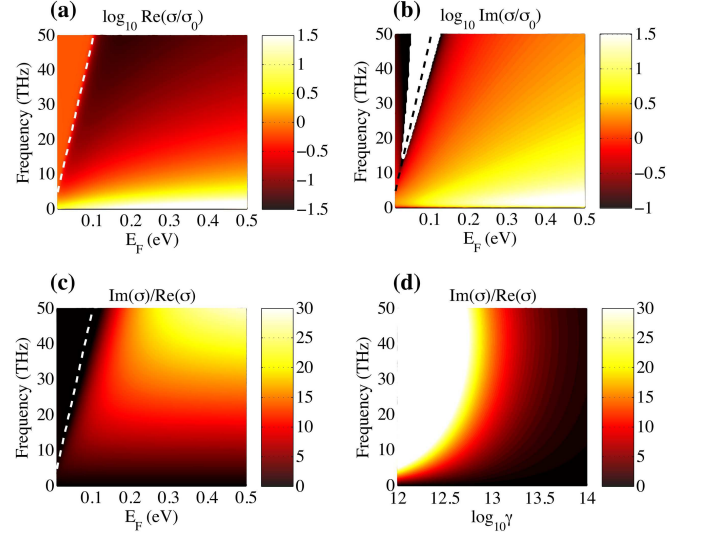


Figure 4. (Color online) Graphene conductivity σ in the units of elementary conductivity $\sigma_0 = e^2/4\hbar = 0.061$ mS in logarithmic scale, (a) real and (b) imaginary part, depending on frequency ω and electrochemical potential (Fermi level) E_F . The dashed line corresponds to the Pauli blocking limit $\hbar\omega = 2E_F$. The white region around the dashed line in (b) corresponds to the region of negative $\text{Im } \sigma$. Also shown is the figure of merit $FoM = \text{Im } \sigma / \text{Re } \sigma$ dependence on frequency and (c) E_F for the damping $\gamma = 10^{13} \text{ s}^{-1}$; (d) on the damping γ for the fixed Fermi level $E_F = 0.2 \text{ eV}$. We consider the regions with $FoM > 10$ suitable for HMMs.

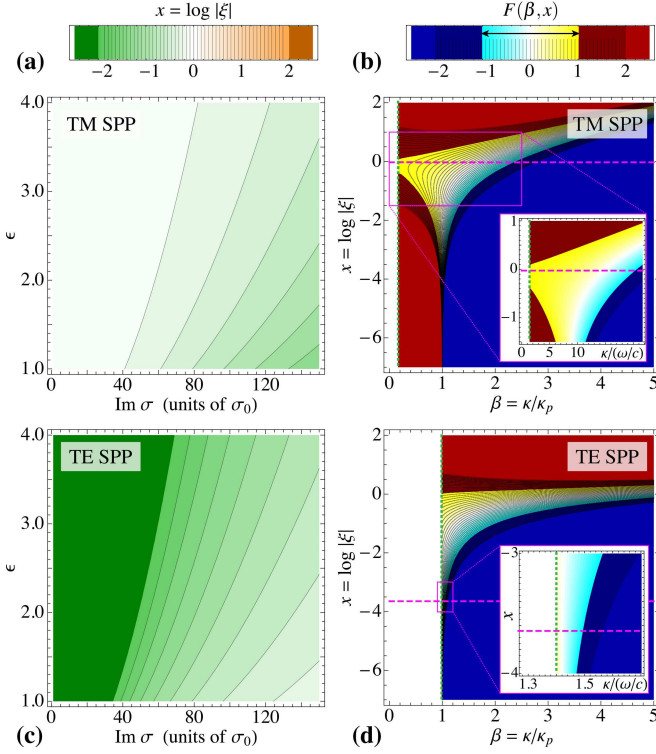


Figure 5. (Color online) Formation of the VPP band in graphene HMMs. (a) The dependence of x on graphene conductivity and dielectric layer permittivity. (b) Same as Fig. 3b for graphene multilayers with $\sigma = 20i\sigma_0$ [where $\sigma_0 = e^2/(4\hbar)$], $d = 5$ nm, and $\varepsilon = 1.96$. (c–d) Same as (a–b) but for TE-polarized graphene plasmons.

introducing $S \equiv 2\varepsilon/(Z_0 \text{Im } \sigma)$, Eq. (23) yields the expressions for the pole expansion coefficients

$$\kappa_p = \sqrt{\varepsilon + S^2}, \quad \tau = -\frac{S^2}{\sqrt{\varepsilon + S^2}}, \quad \xi = -\frac{S^2}{\varepsilon + S^2}. \quad (24)$$

It is remarkable that realistic graphene conductivities in the range $\text{Im } \sigma < 100e^2/(4\hbar)$ yield large values of $S \simeq 1 \dots 100$. Since $|\xi|$ tends to unity for large S , it turns out to be between 0.1 and 1, which is favorable for the VPP band to be broad and pronounced, in a large parameter window, as shown in Fig. 5(a). Changing the Fermi level allow the tuning of conductivity to the desired value [see Fig. 4(b)] while maintaining the deeply subwavelength thickness of such layers for THz frequencies; Figure 5(b) additionally confirms the presence of a VPP band in such graphene-dielectric multilayers.

The key difference between VPPs in metal-dielectric and graphene multilayers is that in the former $\xi \gtrsim 1$ while in the latter $\xi \lesssim 1$. As a result, metal-dielectric layers benefit from a decrease of $\eta\kappa_p$ (e.g., by decreasing d_d and making the structure more subwavelength), whereas for graphene multilayers this is less relevant because the slanted branch of $F(\beta, x) \in [-1; 1]$ is outside of the working values of $x < 0$.

It was also pointed out recently that in addition to conventional SPPs for TM-polarized waves, graphene supports transverse TE-polarized SPPs^{24,25} in a narrow range of parameters where $\text{Im } \sigma < 0$ and $\text{Re } \sigma$ is small. It is interesting to analyze

whether these SPPs can give rise to HMM-like behavior. The TE counterparts to Eqs. (23)–(24) are

$$T' = \frac{2\sqrt{\varepsilon - \kappa^2}}{2\sqrt{\varepsilon - \kappa^2} + (Z_0\sigma)}, \quad (25)$$

and (introducing $Q \equiv Z_0|\text{Im } \sigma|/2$)

$$\kappa'_p = \sqrt{\varepsilon + Q^2}, \quad \tau' = \frac{Q^2}{\sqrt{\varepsilon + Q^2}}, \quad \xi' = \frac{Q^2}{\varepsilon + Q^2}. \quad (26)$$

Here we note that TE-polarized plasmons only exist very close to the singularity point in the graphene conductivity, with realistic $|\text{Im } \sigma| < 1 \dots 2e^2/(4\hbar)$. Hence Q is a small quantity on the order of 0.05, making κ'_p very close to $\sqrt{\varepsilon}$ and $\xi' \ll 1$. This makes TE-polarized plasmons in graphene much like LRSPPs, which only hybridize into an extremely narrow VPP band, as can indeed be seen in Fig. 5(c–d).

C. Influence of losses

It is important to note that in presence of losses, bulk plasmonic waves in the high- k band would acquire an imaginary part, and the difference between propagating waves within the VPP band and evanescent waves outside it becomes less pronounced. For smaller amounts of losses, such as for $\text{Im } \varepsilon_m \ll |\text{Re } \varepsilon_m|$ in better metals, the high- k band can nonetheless be rather well-defined, even though its edges are smeared²⁸, so the conclusions of the present analysis would persist.

However, in graphene there can be conditions when the real part of the conductivity is quite significant [see Fig. 4(a)]. In such cases, the presented results can only be used as a guideline, and the precise characteristics of VPPs should be established by additional calculations.

To define the parameter range where the present analysis is applicable, we introduce the figure-of-merit $FoM = \text{Im } \sigma / \text{Re } \sigma$, which is an adaptation of the quantity commonly used to characterize the amount of losses in metamaterials to a single graphene sheet. We will assume that losses in graphene are small if $FoM > 10$. Figure 4(c) presents the figure-of-merit for the damping value $\gamma = 10^{13} \text{ s}^{-1}$ ³⁵. As we see, $FoM > 10$ corresponds to the Fermi level $E_F > 0.15 \text{ eV}$ and frequencies above 20 THz, whereas in the lower THz and microwave range graphene is essentially just a dissipative layer (resistor). We should keep in mind that at photon energies larger than 0.2 eV, which corresponds to the frequencies above 50 THz, the interaction with the lattice phonons of the dielectric spacer layers in multilayered graphene introduce additional large losses not taken into account in Eq. (22). Therefore the region from 20 to 50 THz is probably the best for the realization of graphene based HMMs, and larger E_F are favorable for better HMM performance.

Another parameter, namely, damping (or collision frequency) γ depends very much on the quality of graphene (its growth process and handling when transferring to the substrate). The values reported in the literature vary from 10^{12} s^{-1} to 10^{14} s^{-1} (the reader is referred to the recent review of

graphene for THz applications³⁵). In Fig. 4(d) the influence of damping on the figure-of-merit is demonstrated. Whereas for the above mentioned $\gamma = 10^{13} \text{s}^{-1}$ graphene could be only used for HMM starting from 20 THz, reducing the damping by 10 times ($\gamma = 10^{12} \text{s}^{-1}$) makes graphene HMMs feasible starting from as low as 1.6 THz. On the other hand, doubling the damping to $\gamma = 2 \times 10^{13} \text{s}^{-1}$ makes graphene useless for building HMMs in the entire THz-IR range. However, there are definite grounds for optimism in the constant progress in graphene fabrication technology. For example, chemical vapor deposition growth of centimeter-large monocrystalline graphene with the quality rivaling that of exfoliated graphene³⁶ and large mobility of carriers in graphene surrounded by two-dimensional boron nitride³⁷ have been reported recently.

V. CONCLUSIONS AND OUTLOOK

In summary, we have investigated the general theoretical conditions for an arbitrary elementary excitation existing in the unit cell of a multilayer periodic system to hybridize into a broadband bulk high- k propagating waves (such as VPPs in HMMs). By isolating the unit-cell elementary excitation in the form of a generalized resonance defined by a pole-like response in its Fresnel reflection and transmission coefficients [Eq. 8], and by using Bloch's theorem to couple the unit cells via dielectric spacer layers, we have derived analytic relations connecting the width of the resulting band of propagating waves in the k -space with the properties of the elementary excitations, such as the pole location and strength, as well as parameters of the dielectric spacer layers.

Using these analytical expressions, we have confirmed that one kind of surface plasmons existing in thin metal layers, namely the SRSPPs, can and normally do give rise to a broad band of volume plasmon polaritons, resulting in HMM-like properties of subwavelength metal-dielectric multilayers¹⁸. Conversely, the other kind of SPPs in such layers, namely the LRSPPs, only form a very narrow plasmonic band near the light line of the dielectric and do not produce a broad high- k band.

We have also applied the formalism to multilayered graphene-dielectric metamaterials in the THz range and shown that TM-polarized plasmons in individual graphene sheets do hybridize to form VPPs with HMM-like properties, and the VPP band is broadband enough for realistic

values of graphene conductivity [for the considered geometry $\text{Im} \sigma < 100e^2/(4\hbar)$]. On the other hand, transverse (TE-polarized) graphene plasmons only form a very narrow VPP band, not giving rise to HMM properties and behaving like LRSPPs in this respect. We have also shown that graphene can be a good building material for high- k band THz and IR metamaterials, if it has sufficiently high quality (the damping γ smaller than $2 \times 10^{13} \text{s}^{-1}$).

Along with providing the general theoretical understanding of the formation of a high- k band of bulk propagating waves from fixed- k surface excitations in individual layers of a multilayer system, our results have promising practical applications. They are twofold. First, the analytic expressions allow for very easy and computationally efficient estimations of VPP dispersion in existing metal-dielectric and graphene multilayer HMMs, which can be used to design HMMs with optimized performance. Second, on a more abstract level, the formalism provides insight into a general question whether broadband large-wavevector higher-dimensional response should be expected from *any* given type of lower-dimensional elementary excitations in *arbitrary* periodic systems, not necessarily bi-layer unit cells, but also many-layer and gradient. Examples may include new types of photonic structures such as waveguide arrays and multilayers based on Bloch surface waves or spoof surface plasmons. Moreover, by virtue of mathematical similarities between electromagnetic waves and other wave phenomena in physics (such as acoustic waves in elastic multilayers and steady-state solutions of the Schrödinger equation in multiple quantum-well heterostructures), it can be speculated that the present results may be applied to these alternative systems, extending the metamaterial approach beyond electromagnetism.

ACKNOWLEDGMENTS

S.V.Z. acknowledges financial support from the People Programme (Marie Curie Actions) of the European Union's 7th Framework Programme FP7-PEOPLE-2011-IIF under REA grant agreement No. 302009 (Project HyPHONE). A.A. acknowledges financial support from the Danish Council for Technical and Production Sciences through the GraTer (0602-02135B) project. J.E. Sipe acknowledges financial support from the Natural Sciences and Engineering Research Council of Canada.

* sezh@fotonik.dtu.dk

¹ Z. Jacob, J.-Y. Kim, G.V. Naik, A. Boltasseva, E. E. Narimanov, and V. M. Shalaev, Appl. Phys. B 100, 215 (2010).

² Z. Jacob, L. V. Alekseyev, and E. Narimanov, Opt. Express 14, 8247–8256 (2006).

³ Z. Jacob, I. I. Smolyaninov, and E.E. Narimanov, Appl. Phys. Lett. 100, 181105 (2012).

⁴ M. A. Noginov, Yu. A. Barnakov, G. Zhu, T. Tumkur, H. Li, and E. E. Narimanov, Appl. Phys. Lett. 94, 151105 (2009).

⁵ M. A. Noginov, H. Li, Yu. A. Barnakov, D. Dryden, G. Nataraj, G. Zhu, C. E. Bonner, M. Mayy, Z. Jacob, and E. E. Narimanov, Opt. Lett. 35, 1863 (2010).

⁶ J. Kim, V. P. Drachev, Z. Jacob, G. V. Naik, A. Boltasseva, E. E. Narimanov, and V. M. Shalaev, Opt. Express 20, 8100–8116 (2012).

⁷ E. E. Narimanov, H. Li, Y. A. Barnakov, T. U. Tumkur, and M. A. Noginov, Opt. Express 21, 14956–14961 (2013).

⁸ I. I. Smolyaninov and E. E. Narimanov, Phys. Rev. Lett. 105,

- 067402 (2010).
- ⁹ I. I. Smolyaninov and Yu-Ju Hung, J. Opt. Soc. Am. B 28, 1591–1595 (2011).
 - ¹⁰ C. L. Cortes, W. Newman, S. Molesky, and Z. Jacob, J. Opt. 14, 063001 (2012).
 - ¹¹ V. Drachev, V. A. Podolskiy, and A. V. Kildishev, Opt. Express 21, 15048–15064 (2013).
 - ¹² J. Schilling, Phys. Rev. E 74, 046618 (2006).
 - ¹³ I. Avrutsky, I. Salakhutdinov, J. Elser, and V. Podolskiy, Phys. Rev. B 75, 241402(R) (2007).
 - ¹⁴ S. Ishii, A. V. Kildishev, E. Narimanov, V. M. Shalaev, and V. P. Drachev, Laser Photon. Rev. 7, 265–271 (2013).
 - ¹⁵ S. Feng, J. M. Elson, and P. L. Overfelt, Opt. Express 13, 4113–4124 (2005).
 - ¹⁶ B. Wood, J. B. Pendry, and D. P. Tsai, Phys. Rev. B 74, 115116 (2006).
 - ¹⁷ G. Rosenblatt and M. Orenstein, Opt. Express 19, 20372–20385 (2011).
 - ¹⁸ S. V. Zhukovsky, O. Kidwai, and J. E. Sipe, Opt. Express 21, 14982 (2013).
 - ¹⁹ A. A. Orlov, P. M. Voroshilov, P. A. Belov, and Yu. S. Kivshar, Phys. Rev. B 84, 045424 (2011).
 - ²⁰ A. Andryieuski, A. V. Lavrinenko, and D. N. Chigrin, Phys. Rev. B 86, 121108 (2012).
 - ²¹ I. V. Iorsh, I. S. Mukhin, I. V. Shadrivov, P. A. Belov, and Yu. S. Kivshar, Phys. Rev. B 87, 075416 (2013).
 - ²² K. V. Sreekanth, A. De Luca, and G. Strangi, Appl. Phys. Lett. 103, 023107 (2013).
 - ²³ M. A. K. Othman, C. Guclu, and F. Capolino, Opt. Express 21, 7614–7632 (2013).
 - ²⁴ S. A. Mikhailov and K. Ziegler, Phys. Rev. Lett. 99, 016803 (2007).
 - ²⁵ M. Jablan, H. Buljan, and M. Soljačić, Opt. Express 19, 11236–11241 (2011).
 - ²⁶ A. Yariv and P. Yeh, *Optical Waves in Crystals* (New York: Wiley, 1983).
 - ²⁷ X. Ni, S. Ishii, M. D. Thoreson, V. M. Shalaev, S. Han, S. Lee, and A. V. Kildishev, Opt. Express 19, 25242–25254 (2011).
 - ²⁸ O. Kidwai, S. V. Zhukovsky, and J. E. Sipe, Phys. Rev. A 85, 053842, (2012).
 - ²⁹ W. Yan, M. Wubs, and N. Asger Mortensen, Phys. Rev. B 86, 205429 (2012).
 - ³⁰ R. M. Corless, G. H. Gonnet, D. E. G. Hare, D. J. Jeffrey, and D. E. Knuth, Adv. Comput. Math. 5, 329–359 (1996).
 - ³¹ O. Kidwai, S. V. Zhukovsky, and J. E. Sipe, Opt. Lett. 36, 2530 (2011).
 - ³² Z. Xu, C. Chen, S. Qing Yang Wu, B. Wang, J. Teng, C. Zhang, and Q. Bao, Proc. SPIE 8923, 89230C (2013).
 - ³³ G. Hanson, J. Appl. Phys. 103, 064302 (2008).
 - ³⁴ A. Andryieuski and A. V. Lavrinenko, Opt. Express 21, 9144–9155 (2012).
 - ³⁵ P. Tassin, T. Koschny, C. Soukoulis, Science 341, 620–621 (2013).
 - ³⁶ Y. Hao, M. S. Bharathi, L. Wang, Y. Liu, H. Chen, S. Nie, X. Wang, H. Chou, C. Tan, B. Fallahazad, H. Ramanarayan, C. W. Magnuson, E. Tutuc, B. I. Yakobson, K. F. McCarty, Y.-W. Zhang, P. Kim, J. Hone, L. Colombo, and R. S. Ruoff, Science 342, 720 (2013).
 - ³⁷ L. Wang, I. Meric, P. Y. Huang, Q. Gao, Y. Gao, H. Tran, T. Taniguchi, K. Watanabe, L. M. Campos, D. A. Muller, J. Guo, P. Kim, J. Hone, K. L. Shepard, and C. R. Dean, Science 342, 614 (2013).